

Fabrication of Low-Loss GaN/AlN Waveguides for Nonlinear Optics

Aydin Akyurtlu

Bradley Department of Electrical & Computer Engineering, Virginia Polytechnic Institute & State University

NNIN REU Site: Cornell NanoScale Science & Technology Facility, Cornell University

NNIN REU Principal Investigator: Dr. Farhan Rana, Department of Electrical and Computer Engineering, Cornell University

NNIN REU Mentor: Jahan Dawlaty, Department of Electrical and Computer Engineering, Cornell University

Contact: aakyur08@vt.edu, farhan.rana@cornell.edu, jd234@cornell.edu

Abstract

Nonlinear optical phenomena have well-established applications in many areas, such as optical telecommunications. Through the fabrication of low loss waveguides at micron length scales, such nonlinear phenomena can be scaled for use in integrated device applications. The purpose of this research was to fabricate gallium nitride / aluminum nitride (GaN/AlN) waveguides on sapphire substrates that demonstrate low loss and observable nonlinear effects. Because nonlinear effects require very high intensity, mode confinement becomes a very important factor. To increase mode confinement in the fabricated waveguides, a potassium hydroxide (KOH) wet etch is used to undercut the AlN base, increasing mode confinement in GaN. Waveguides were fabricated on sapphire wafers with molecular beam epitaxy (MBE)-grown GaN/AlN layers using standard photolithography and dry etching techniques yielding features ranging from 2-5 μm in width. The waveguides were tested using a femtosecond laser system.

Introduction and Background

Optoelectronic and photonic devices are a class of semiconductor devices that utilize and process light signals. One of the primary components of many of these devices is waveguides that are used to guide the light signals within the device. For device efficiency and information integrity, it is important that waveguides exhibit very low scattering losses. While the guiding properties of waveguide structures are very important to the functioning of such devices, waveguides can also be used to process optical signals through the use of nonlinear optical effects. At very high intensities, such as those provided by a laser, the polarization of the guiding medium interacts nonlinearly with the incident field in ways that are modeled using a power series representation of the electrical susceptibility with terms exceeding linear order. These nonlinearities give rise to many interesting phenomena, such as second and third harmonic generation, sum frequency generation, and Raman shifting. Nonlinear effects are already utilized in macroscale waveguiding structures such as optical fibers. Because nonlinear effects only become pronounced at high intensities, loss and mode confinement become critical properties that must be optimized.

Waveguide Fabrication

The wafers used for manufacturing were 3" sapphire wafers with various epitaxially grown III-V layers. The two layer types used were; (1) a 500 nm AlN layer with alternating layers of GaN/AlN quantum wells and (2) a 1.4 mm bulk GaN layer on top of 100 nm bulk AlN. A thick layer of silicon dioxide (SiO_2), $\sim 1 \mu\text{m}$, was deposited on the wafer using pressure-enhanced chemical vapor deposition (PECVD) to act as a more robust mask for the III-V dry etch process. After standard photolithography using a

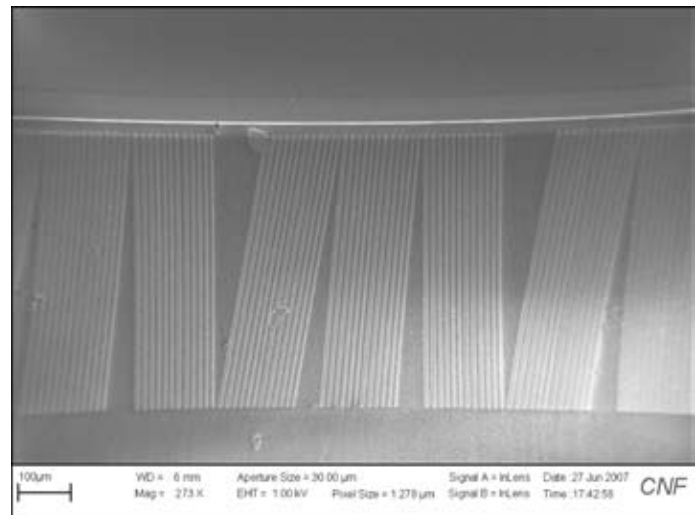


Figure 1: Row of fabricated waveguides.

10x i-line stepper for exposing, the SiO_2 layer was etched using a CHF_3/O_2 dry etch chemistry in a reactive ion etcher (RIE). The III-V layers were etched using an $\text{Ar}/\text{BCl}_3/\text{Cl}_2$ RIE dry etch in an ICP etcher. The samples were finally treated with resist stripper and HF to remove the photoresist and SiO_2 masking layers. With minimal optimization, the process was found to achieve good sidewall smoothness for features $\geq 3.5 \mu\text{m}$, but there was noticeable damage during the nitride etch process to $2 \mu\text{m}$ and $2.5 \mu\text{m}$ features. Increased sidewall smoothness and reduction in damage to small features could most likely be improved by utilizing a thicker oxide mask layer and further optimization of the III-V etch process.

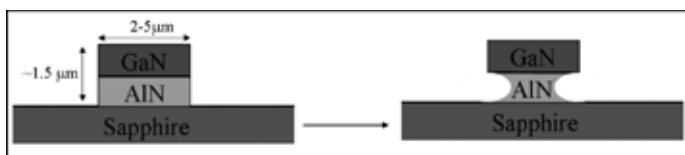


Figure 2: Diagram of KOH undercut.

KOH Undercut

In order to increase the nonlinear effects in the waveguides, an undercut in the lower AlN layer of the bulk GaN/AlN waveguides was created. The undercut would reduce the cross-sectional area of the AlN layer, which would cause the mode to be confined more strongly in the GaN layer, reducing mode volume. Previous research [1,2] had indicated that KOH solutions were capable of selectively etching AlN over other III-V compounds. Waveguides fabricated in the bulk GaN/AlN sample were treated in heated AZ400K developer for 30 minutes at $90^{\circ}\text{C} \pm 5^{\circ}\text{C}$. The solution selectively etched the AlN over the GaN such that a noticeable undercut was formed. A rough scanning electron microscopy (SEM) measurement showed the etch rate to be very approximately 20 nm/min.

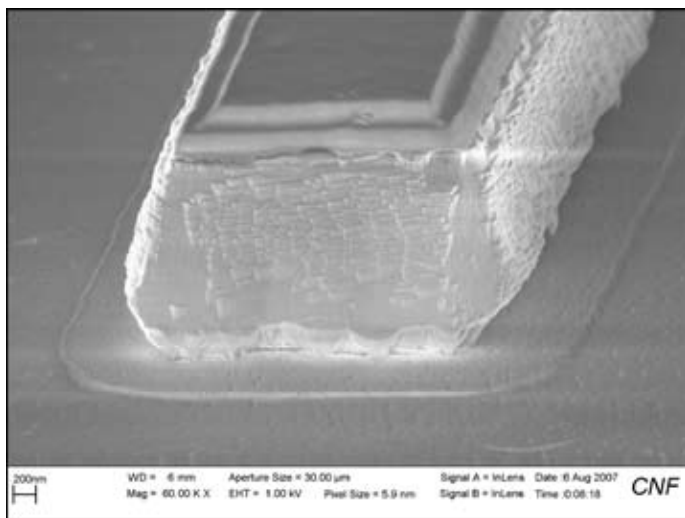


Figure 3: Profile of bulk GaN/AlN waveguide with KOH undercut.

Testing Results and Conclusions

Testing the fabricated waveguides was accomplished using a bright white light source generated by nonlinear interaction of a pulsed fiber laser with a photonic crystal fiber. The laser was coupled to the waveguide by focusing the beam through a lens and the output was observed using a CCD. Only qualitative data could be taken due to equipment and time limitations. The CCD was used to capture various mode profiles for qualitative comparison of waveguides with different

material composition and fabrication processes. Comparison of mode profiles in the three tested samples is shown in Figure 4. All fabricated waveguides were shown to support guided modes, but exhibited visible scattering loss. Due to the conservative undercut and significant surface scattering at the facet, there was no concrete difference in mode confinement between the bulk GaN waveguides with and without undercutting, but the initial results show enough potential to warrant further study.

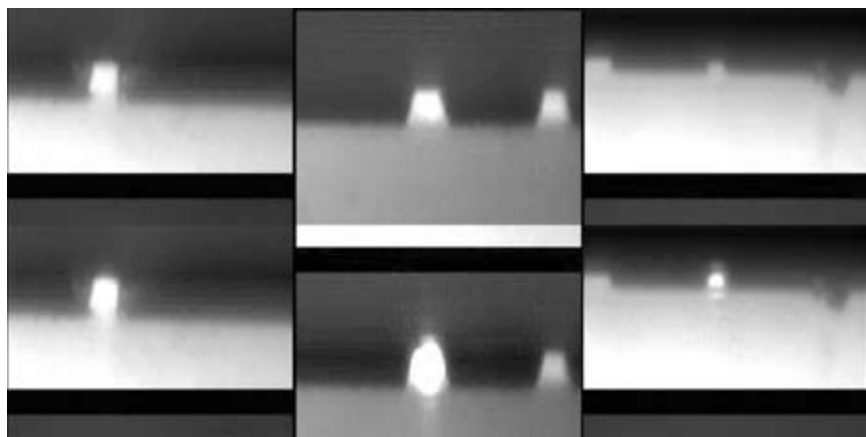
Acknowledgements

I would like to thank Dr. Farhan Rana and Jahan Dawlaty, as well as everyone in the Rana Group, for their help in this project. I would like to thank the entire CNF staff for their assistance in making the technical side of my project possible. I would also like to thank Melanie-Claire Mallison, Lynn Rathbun, the NSF, and the National Nanotechnology Infrastructure Network Research Experience for Undergraduates Program for coordinating this program and giving me this opportunity.

References

- [1] Mileham, J.R.; Pearton, S.J.; Abernathy, C.R.; Mackenzie, J.D.; Shul, R.J.; Kilcoyne, S.P.; "Patterning of AlN, InN, and GaN in KOH-based solutions."; *Journal of Vacuum Science & Technology A: Vacuum, Surfaces, and Films*; Volume 14; Issue 3, May 1996; pp. 836-839.
- [2] Simeonov, D.; Feltin, E.; Buhlmann, H.-J.; Zhu, T.; Castiglia, A.; Mosca, M.; Carlin, J.-F.; Butte, R.; Grandjean, N.; "Blue lasing at room temperature in high quality factor GaN/AlN microdisks with InGaN quantum wells."; *Applied Physics Letters*; Issue 90 (2007).

Figure 4: Guide and mode profiles. From left to right: Bulk GaN/AlN with undercut, Bulk GaN/AlN without undercut, Bulk AlN with GaN/AlN quantum wells.



Quantum Dot Light Emitters

Rehan Kapadia

Electrical Engineering, University of Texas at Austin

NNIN REU Site: Minnesota Nanotechnology Cluster, University of Minnesota-Twin Cities

NNIN REU Principal Investigator: Dr. Steven Campbell, Electrical Engineering, University of Minnesota-Twin Cities

NNIN REU Mentor: Gagan Aggarwal, Electrical Engineering, University of Minnesota-Twin Cities

Contact: Kapadia.rehan@gmail.com, campb001@umn.edu, aggar014@umn.edu

Abstract

Quantum confinement effects allow radiative recombination of holes and electrons in silicon nanoparticles (NP), also referred to as quantum dots (QD). This is an area of considerable interest as QDs have the potential for high efficiency, and have the ability to tune the emission wavelength with the QD size. Currently, devices use organic polymers to inject holes and electrons onto the QDs, where 1-2% radiatively recombine. Inorganic materials are generally deposited at elevated temperature. The low thermal stability of QDs result in a belief that they are incompatible with inorganics. The objective of the current approach is to demonstrate how a layer of QDs behaves when trapped between two inorganic materials. To test the photoluminescence (PL), we deposited QDs on silicon nitride and used atomic layer deposition (ALD) to grow a thin layer of hafnium oxide (HfO_2) at very low temperature. The PL was measured after deposition of QDs and HfO_2 . Results show no degradation in PL intensity. For electroluminescence (EL) measurements, we used a structure of ITO-ZnO-QDs-AlN-Pt. The silicon NPs used were generated by decomposition of silane in plasma and were directly deposited onto the substrates. The devices were created by ALD deposition of zinc oxide (ZnO) on an indium tin oxide (ITO) covered glass slide and sputtering of the aluminium nitride (AlN) onto the QD-ZnO-ITO layers.

Introduction

We can exploit the quantum confinement effects in quantum dots (QDs) to cause photoluminescence (PL) and electroluminescence (EL). Current direct-gap inorganic light emitting diode (LED) technology is efficient but expensive. The organic LEDs used today have reliability problems as well as poor color depth. By using QDs as the electroluminescent element, we can tune the emission wavelength and potentially create high efficiency reliable EL devices. Presently, to conduct electrons and holes to the QDs, organic polymers are used as the electron and hole conducting layers. The use of these materials presents many of the same stability problems seen in organic light emitters. We will attempt to use inorganic materials instead.

Experimental Procedure

The focus of this project was two-fold. First, we must determine if the intensity of the PL of QDs is reduced when sandwiched between inorganic materials. This will allow us to determine whether the quantum confinement effects or the crystalline structure of the QDs are damaged. Second, we must find if electroluminescent devices can be created using only inorganic materials.

The device to test the PL was fabricated on a glass slide that was covered with ITO. The structure, as shown in Figure 1a, was plasma enhanced chemical vapor deposition (PECVD) Si_3N_4 , a layer of QDs, and ALD HfO_2 . The Si_3N_4 layers were between 60Å and 90Å, grown at a rate of 75Å/min. The QDs were

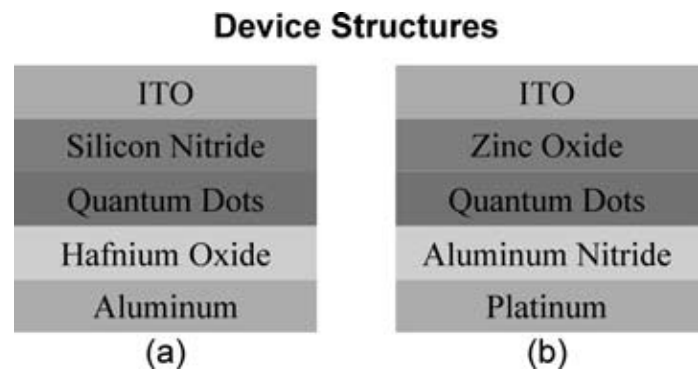


Figure 1

deposited by placing the samples in the exhaust stream of the plasma where the QDs were formed. The samples were placed in the exhaust stream for 30s, 45s, 1 min, 2 min, 3 min, 4 min and 6 min. Following QD deposition, 60Å of HfO_2 were grown on the samples by ALD at 130°C using trimethyl aluminum and water. The PL was tested after both the QD deposition and the ALD.

To test the EL, the device shown in Figure 1b was fabricated. 70Å of ZnO was deposited at 250°C on the ITO covered glass slide using ALD. The QDs were deposited in a similar fashion as the first set of devices. The layer of AlN was sputtered for 1 min using an Al target and N_2 in the environment. Platinum electrodes were then sputtered on top of the AlN.

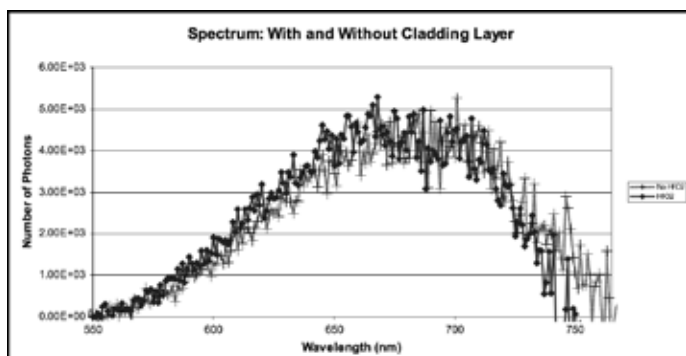


Figure 2

Results and Conclusions

The spectrums of the $\text{Si}_3\text{N}_4/\text{HfO}_2$ devices, shown in Figure 2, indicate that there was no noticeable change in intensity of the PL after HfO_2 deposition. The tests were run under the same conditions, so that the magnitudes of the spectrums were comparable. This indicates that the crystalline structure and the quantum confinement effects of the QDs were intact. Thus, ALD growth methods can now be used to create novel device structures.

The ZnO/AlN devices should have behaved as a diode due to the band alignment. However, the I-V curves in Figure 3 show that the behavior was ohmic. We believe there were pinholes in the thin sputtered films, causing all the current to flow through only one material and to be localized near the pinholes. This also would explain why no EL was observed. None of the current went through the QDs. When a constant voltage was applied to the devices and the devices were excited by UV light, PL was clearly visible, but the current flowing through the device did not appreciably change.

These results do not rule out the possibility that inorganic layers may be used as electron and hole transport layers. However, the films that were grown over the QD layer were only characterized using ellipsometry and profilometry on test wafers. This does not tell us what types of films were actually being grown on the QDs. Therefore, the results indicated that the structure of the devices were not as expected. Due to the extreme uniformity of ALD layers, we suspect that the pinholes were in the sputtered films, although this has yet to be proven.

Future Work

Since the quality of the films appeared to be a problem, careful study of the nucleation and growth of films on quantum dots needs to be pursued. The layer of QDs should also be characterized, as it would allow us to determine what type of surface we are depositing the materials onto. There should also be tests on control substrates so we can determine what thickness of materials are necessary to reliably give us diode characteristics.

Acknowledgments

I would like to thank my PI, Dr. Campbell, as well as graduate students in his group: Gagan Aggarwal, Rick Liptak, and Sang Ho Song, and postdoctoral fellow, Dr. Xiaodong Pi. I would also like to thank University of Minnesota, National Nanotechnology Infrastructure Network Research Experience for Undergraduates Program, and NSF.

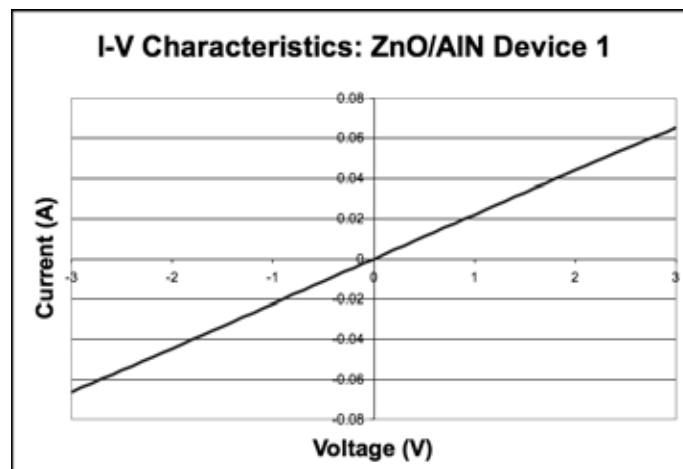


Figure 3

Characterization and Optimization Study of Silicon Evanescent Racetrack Lasers

Brian McSkimming

Electrical & Computer Engineering, University at Buffalo, State University of New York

NNIN REU Site: Nanotech—The UCSB Nanofabrication Facility, University of California, Santa Barbara

NNIN REU Principal Investigator: Dr. John Bowers, Electrical and Computer Engr., University of California, Santa Barbara

NNIN REU Mentor: Alexander Fang, Electrical and Computer Engineering, University of California, Santa Barbara

Contact: bmm6@buffalo.edu, bowers@ece.ucsb.edu, awfang@ece.ucsb.edu

Introduction

The electrically pumped hybrid silicon evanescent laser has been presented as a novel device which satisfies the desire to manufacture low cost, high volume silicon lasers with the goal of using photonic circuitry to replace traditional metal interconnects for board to board and chip to chip applications. The hybrid silicon evanescent device platform has already been demonstrated in the form of a photodetector, an optical amplifier and a racetrack laser [1]. The silicon evanescent laser is achieved through bonding a III-V multiple quantum well (MQW) active layer structure to a silicon waveguide. For efficient current flow to the active region, protons are implanted into the cladding layer of the III-V structure in order to prevent lateral carrier diffusion and thereby increasing the current and optical mode overlap in the quantum wells.

We report here the optimization of this proton implant profile for two laser characteristics, threshold lasing current and device capacitance, and show an improvement of both these characteristics. This technique was implemented and used in the design of the silicon evanescent laser in an attempt to maximize the injection efficiency into the MQW active layer. Injection efficiency is the fraction of injected carriers which contribute to light generation, is one factor used to characterize lasers. Another factor which can affect performance of the silicon evanescent laser is the capacitance between the n contact layer and the p contact layer.

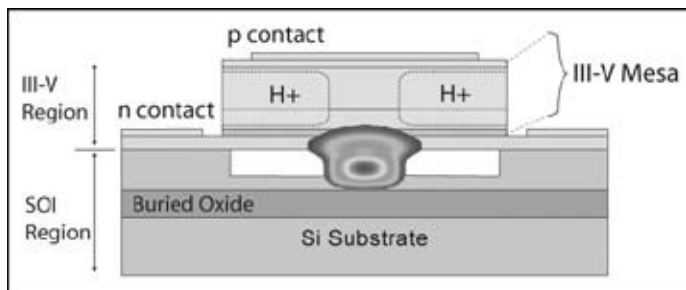


Figure 1: Cross-sectional illustration of device platform.

Device Structure/Fabrication

The silicon evanescent laser device platform consists of two separately regions bonded together. Figure 1 is an illustration of the cross-sectional view of the device. The top portion is a III-V heterostructure consisting of a n-region, multiple quantum well (MQW) active region and p-cladding region which are epitaxially grown on an indium phosphide (InP) substrate. The bottom portion is a silicon waveguide structure processed from a silicon-on-insulator (SOI) substrate. The two pieces are bonded using a low temperature O₂ plasma assisted wafer bonding technique [2]. The InP is then etched using both reactive ion etching (RIE) through the p region, and wet etching through the MQW to create a mesa ~ 10 μm wide in order to access the n layers. n and p contact pads are subsequently deposited and annealed in

forming gas. The sides of the mesa are implanted with protons of varying energies in order to allow for efficient current flow as well as preventing lateral current diffusion. Detailed descriptions of the fabrication process of the hybrid silicon evanescent laser can be found in [3].

An illustration of the silicon evanescent racetrack laser device topography is shown in Figure 2. It consists of a racetrack resonator, two integrated photodetectors, and a directional coupler, which couples light from the resonator and directs it towards the photodetectors.

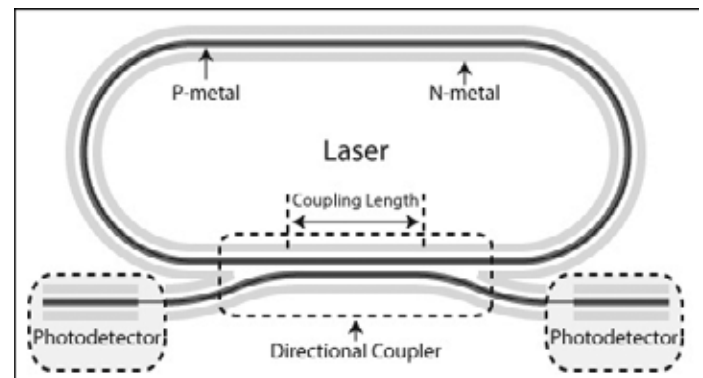


Figure 2: Illustration of silicon evanescent racetrack laser.

Experimental Procedure

This experiment used two different proton implantation profiles, the first being the standard baseline implantation profile as shown. The second implantation profile increased the depth of the protons to correspond to the top of the MQW active region while increasing the height of the protons implanted to correspond to the top of the mesa. By increasing the depth of the implantation to the top of the MQW active region, we intended to improve the injection efficiency into the active region directly above the silicon waveguide. Bringing the implantation profile to the top of the mesa is intended to reduce the capacitance between the p and n layers by decreasing the available area which is behaving as a parallel plate capacitor, in particular the highly doped P-InGaAs contact layer.

During testing, the laser was driven from 0-500 mA in 25 mA increments through the top p-contact. The photodetectors were reverse biased at -5V, and the current across them is measured as the driving current is increased. In order to determine the effect which the deeper proton implant profile has on the injection efficiency, we compared devices implanted with the two different profiles based upon their lasing threshold current. The capacitances of the devices were measured directly.

Results and Conclusions

Eight devices from each profile were tested and analyzed. Using the L-I (Power vs. Current) curve taken from the silicon evanescent racetrack lasers, the lasing threshold current can be determined experimentally. As a result of increasing the proton implant depth the lasing threshold current decreased. Devices 2-4, with a directional coupler length of 100 μm , demonstrated a 17.31% improvement in the average threshold current for proton implant profile 2 over profile 1. As can be seen in Figure 3, the average threshold current for devices 2-4 improved from ~ 192 mA,

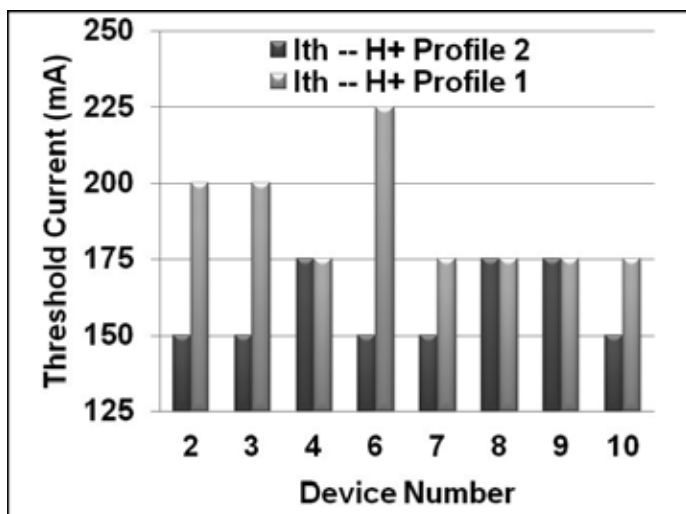


Figure 3: Threshold current comparison between proton implant profiles.

for proton implant profile 1 to ~ 158 mA for proton implant profile 2. Devices 6-10, with a directional coupler length of 300 μm , demonstrated a 4.71% improvement in the average threshold current for proton implant profile 2 over profile 1. The average threshold current for devices 6-10 improved from ~ 175 mA, for proton implant profile 1, to ~ 167 mA for proton implant profile 2. This decrease in the threshold current for these devices demonstrates that the injection efficiency was in fact improved by increasing the depth of the proton implant profile.

As can be seen in Figure 4, the capacitance decreased from an average of ~ 4.6 pF to ~ 3.6 pF with the increase in proton implant height. Overall there was a 21.4% decrease in the capacitances measured for the devices.

Acknowledgements

Thanks to Alex, Dr John Bowers and his group, Intel, and all the supporters of the Bowers Lab. Special thanks to the National Nanotechnology Infrastructure Network Research Experience for Undergraduates Program for this opportunity and to the NSF for funding.

References

- [1] A. W. Fang, et al., "Hybrid Si evanescent devices" *Materials Today* 10, 7-8, (2007).
- [2] D. Pasquariello, et al. "Plasma-Assisted InP-to-Si Low Temperature Wafer Bonding," *IEEE J. Sel. Top. Quantum Electron.* 8, 118, (2002).
- [3] A. W. Fang, et al., "Electrically pumped hybrid AlGaInAs-silicon evanescent laser," *Opt. Express* 14, 9203-9210 (2006).

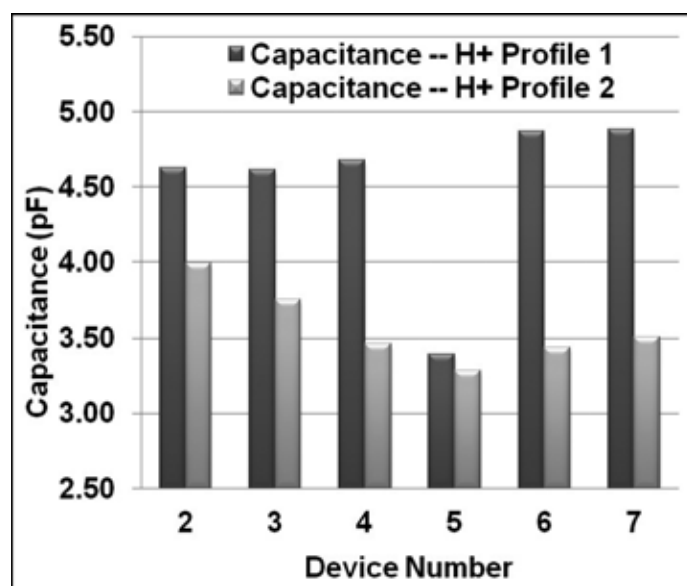


Figure 4: Capacitance comparison between proton implant profiles.

Observation of Harmonics in a Uni-Directional Mode-Locked Fiber Laser Incorporating a Carbon Nanotube Saturable Absorber

Zachary Nishino

Physical Science, St. John's University

NNIN REU Site: Nanoscience at the University of New Mexico

NNIN REU Principal Investigator: Ravi Jain, Electrical & Computer Engineering/Physics, University of New Mexico

NNIN REU Mentor: Li Wang, Electrical & Computer Engineering; Alex Braga, Physics & Astronomy; University of New Mexico

Contact: zachary.nishino06@stjohns.edu, ravijain@unm.edu, liwang@unm.edu

Abstract

The relationship between peak power, pump power, pulse width, spectral width, and repetition frequency with respect to the various harmonics was studied in a uni-directional mode-locked fiber laser incorporating a carbon nanotube saturable absorber. The saturable absorber, which was designed to work at 1550 nm, was composed of 0.8-nm-diameter carbon nanotubes. This laser produced a fundamental frequency of 11.23 MHz, of which the harmonics were multiples. By varying the pump power, an increasing linear relationship developed between repetition frequency and harmonic. We also observed a decreasing linear relationship between spectral width and peak power with the harmonic.

Introduction

Carbon nanotubes exhibit many interesting physical, electrical, thermal, and optical properties. Recently, an interest in their optical properties has made them the point of interest for mode-locked lasers. Due to their fast recovery times, nonlinear absorption of light intensity, and relatively easy fabrication, these nanosized carbon tubes make for a suitable saturable absorber in fiber lasers [1-3]. Coupled with harmonic mode locking, the equal spacing of pulses within the laser cavity, these lasers can be used in optical communication systems for ultra fast data transfer [4-6]. In this experiment, we studied the characteristics of harmonics in a passively mode-locked fiber laser with a carbon nanotube saturable absorber (CNSA).

Experimental Procedure

A uni-directional ring laser cavity was designed with components and measurements as labeled in Figure 1. A fiber pigtailed 980 nm diode (capable of > 100 mW output) was used to pump the 4 meter long erbium doped fiber (EDF). An isolator (> 30 dB isolation) was put in the cavity to ensure uni-directional lasing. A 15 meter long standard single mode fiber was used to compensate the dispersion. The laser was coupled out the cavity through an 88/12 coupler. The carbon nanotube saturable absorber was provided from SouthWest Nanotechnologies and consisted of 0.8-nm-diameter carbon nanotubes. Through the laser output, we utilized a spectrum analyzer to measure the spectrum and spectral width. A digital oscilloscope was used to measure the repetition frequency and to estimate the peak power.

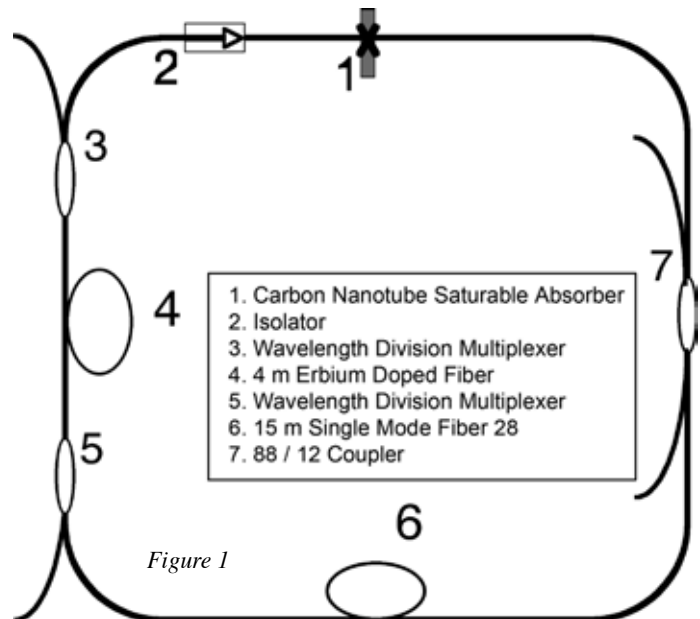


Figure 1

Results

This mode-locked laser operated at a fundamental frequency of 11.23 MHz, of which the harmonics were multiples. Depending on the pump power, the laser operated at different harmonics (up to 14th), see Figure 2. It is almost a linear relationship between the pump power and order of harmonics.

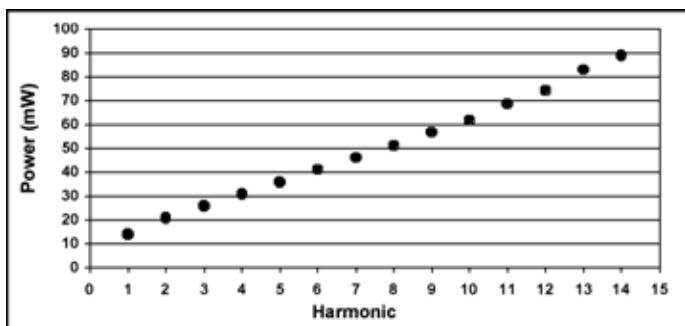


Figure 2

This is the first time that such stable and controllable harmonics have been observed in experiments in such fiber lasers.

To verify that pulses from our laser were from the mode-locked operation instead of another mechanism, like oscillation relaxation or Q-switching, pulse width measurement of the laser was attempted. Although we were not able to determine the actual pulse width from an auto-correlation measurement, we did use the spectrum analyzer to have a preliminary study of the pulse width. The 3-dB widths of the spectra were about 15-16 nm (see Figure 3), depending on the order of harmonics at which the laser was operating.

Directly from $\Delta v \times \Delta t \approx 1$ and $\Delta v/v = \Delta\lambda/\lambda$, it was easy to estimate the pulse width was on the order of 500 fs, which was much smaller than expected for oscillation relaxation or Q-switching. From Figure 3, it was also observed that the overall spectral width decreased (implying the pulse width increased) with increasing harmonics, which has also been observed by other researchers.

Finally, peak powers at different harmonics were measured (see Figure 4). The majority of the data followed a trend of declining as the harmonic increased, which has also been observed by other researchers. However a small section of data developed a trend of slightly increasing as the harmonic increased. This was more than likely due to a change in the digital oscilloscope's settings while the data was being taken.

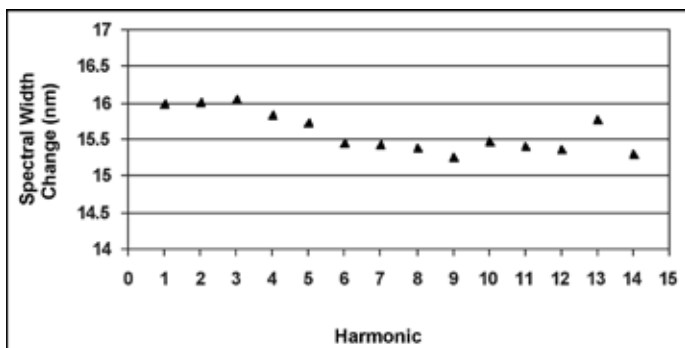


Figure 3

Conclusion

We have demonstrated harmonic mode-locking in a fiber laser incorporating carbon nanotubes. For the first time, it has been demonstrated that reliable harmonics can be tuned by changing the pump power of the laser. Spectral width has been measured to estimate the actual pulse width of the laser.

Acknowledgements

I would like to thank the National Nanotechnology Infrastructure Network Research Experience for Undergraduates and the National Science Foundation for this opportunity. I would like to thank my professor R. K. Jain, my mentors Li Wang and Alex Braga. I would like to make special mention of Jeff Nicholson for his help.

References

- [1] L. Vivien, D. Riehl, and P. Lancon et al. *Optics Lett.* 26, 223 (2001).
- [2] Sze Y. Set, Hiroshi Yaguchi, Yuichi Tanaka, and Mark Jablonski, *J. Lightwave Technology* 22, 51 (2004).
- [3] J. W. Nicholson, "Optically assisted deposition of carbon nanotube saturable absorbers." OFS Laboratories (2006).
- [4] A. N. Pilipetskii, E. A. Golovchenko, and C. R. Menyuk, *Optics Lett.* 20, 907 (1995).
- [5] A. B. Grudinin and S. Gray, *J. Opt. Soc. Am. B* 14, 144 (1997).
- [6] Bülend Ortaç, Ammar Hideur, and Marc Brunel, *Optics Lett.* 29 (2004).

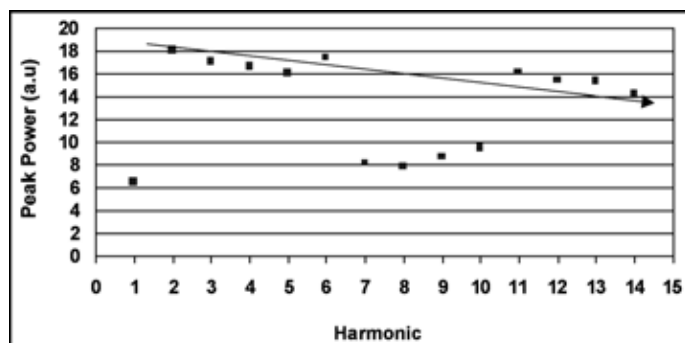


Figure 4

On-Chip Microfluidic Integration of Ultra-High Quality Silicon Optical Microdisk Resonators for Lab-On-Chip Applications

William J. Roman

Biomedical and Electrical Engineering, University of Rhode Island

NNIN REU Site: Microelectronics Research Laboratory, Georgia Institute of Technology

NNIN REU Principal Investigator: Dr. Ali Adibi, Electrical and Computer Engineering, Georgia Institute of Technology

NNIN REU Mentor: Dr. Siva Yegnanarayanan, School of Electrical and Computer Engineering, Georgia Institute of Technology

Contact: roman.will@gmail.com, ali.adibi@ece.gatech.edu, sivay@ece.gatech.edu

Abstract

Silicon on insulator (SOI) technology platform enables the dense monolithic integration of planar nanophotonic optical components and electronic devices. Applying SOI technology to optical sensing, lab-on-chip applications can be envisioned that test for virtually any biomolecule. This project focuses on the design, fabrication, and testing of polydimethylsiloxane (PDMS) channels filled with varying refractive index oils that induce a shift in the resonance wavelength of ultra-high quality (Q) planar microresonators fabricated on SOI substrate, in order to create an effective biosensor. Detection of specific chemical and biological molecules through suitable selective surface coatings on such resonators allows for the rapid, inexpensive production of label-free sensor architectures for lab-on-chip systems [1].

Introduction

SOI substrates offer ultra-compact, ultra-high Q nanophotonic components that are completely compatible with silicon (Si) VLSI technology. Monolithic optical resonators in such SOI substrates, offer the further advantage of micron-scale size, and through suitable designs of the waveguide-cavity coupling, a complete 100% transmission of energy from the waveguide to the cavity is possible. Any molecule present over the resonator is sensed through the resonance wavelength shift induced by the refractive index of the molecule. Successful detection of indices leads to the development of an ultra-compact label-free biosensor.

Experimental Procedure

SOI resonator chips were developed with several add-drop and single disk and ring resonators on each chip for comparison and finding optimal wavelength shifts. PDMS (Sylgard 184) fluidic channels with punched inlet and outlet ports were activated with O₂ plasma and aligned under a microscope to cover the resonators, ensuring index changes (Figure 1). Refractive index oils (Cargille Laboratories) ranging from index 1.32 through 1.395 were individually injected into the channel through a 23-gage polyethylene tubing (Intramedic Clay Adams) using syringes (Norm-Ject 5mL). Each micro-resonator covered with oil from the channel was evaluated for performance using a swept-wavelength test setup that recorded the resonances over a given group of wavelengths. The setup consisted of a tunable laser (Agilent Technologies Model 81680A, line width 100 kHz) for the wavelength sweep, a standard objective lens (Newport M-40x, 0.65NA) for input/output coupling to the device, followed by a photoreceiver (Thorlabs PDB 150C) that was interfaced to a personal computer through a data acquisition (DAQ) card (National Instrument PCI-6251, 16-Bit, 1 MS/s). All light coupled to the resonators used TE-polarized light (Figure 2).

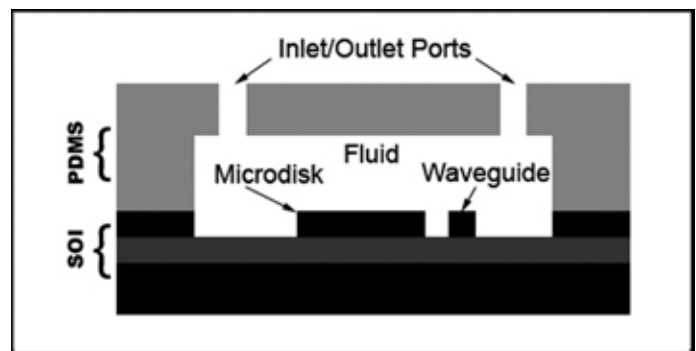


Figure 1: Resonator integrated with microfluidic channel. (Resonator radius: 20 μm , height: 230 nm.)

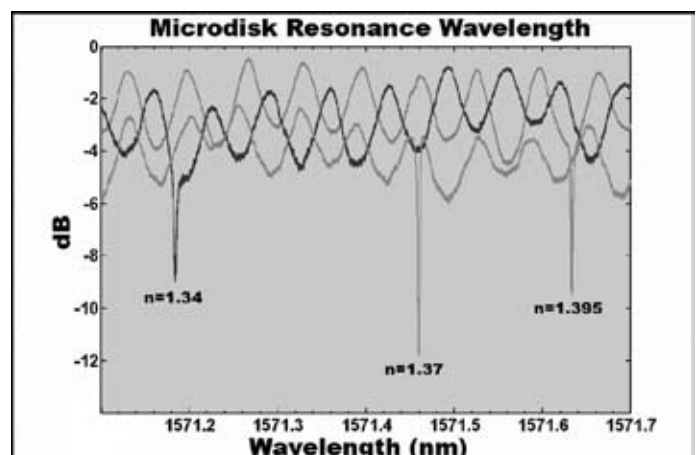


Figure 2: Microdisk spectral response.

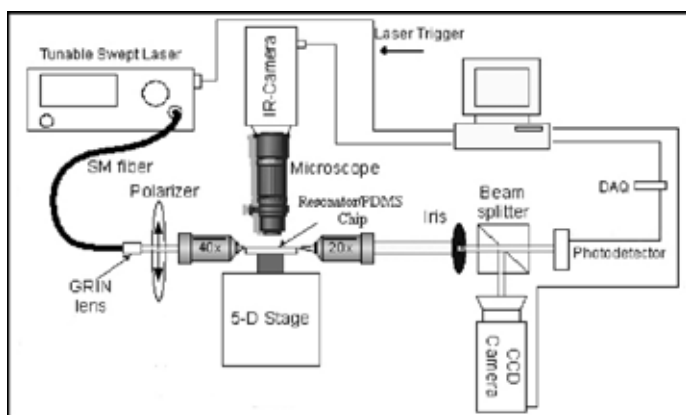


Figure 3: Test setup.

Initial tests of microdisk resonators yielded promising results with high quality factors ($Q > 10^6$; $Q = \lambda/\Delta\lambda$) and noticeable shifts between indices (Figure 3). Microrings, however, yielded greater shifts and were pursued in further tests due to the ease of detecting the index changes (Figure 4).

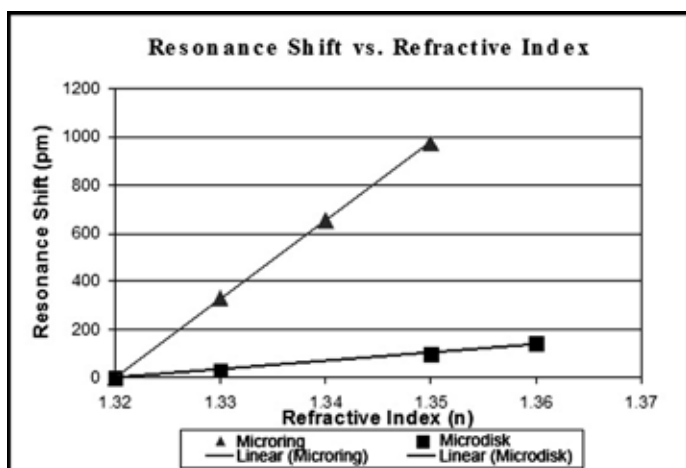


Figure 4: Resonator performance.

Some leaking was observed to come from the bottom of the channel, indicating a poor seal that resulted in a progressive difficulty in coupling the waveguides to the laser to begin the experiment. The imperfect seal resulted in a new channel designs with larger contact areas between the PDMS and Si. After new channel fabrication, real-time data acquisition methods were explored to simulate real-time detection. It was found that by applying a weight to an inverted syringe in a test tube rack (Lake Charles Manufacturing), gravity provided a linear flow rate in the range of $1 \mu\text{L/s}$, suitable for further experimentation and easy index switching.

To rapidly identify indices in real-time, the DAQ program was revised to sweep 10 nm, thereby covering the free-spectral range

of the resonator and hence capturing two resonances. Real-time detection resulted in 350 pm shifts between 0.01 index changes. Repeated measurements revealed that resonance wavelengths were consistent to within 1 pm, for the same index oil under flow conditions. However, it was observed during the real-time tests that the introduction of fluid flow, through applied pressure on the syringe, caused the resonance wavelengths to shift higher by up to 10 pm, when compared to the no-flow condition.

In order to understand this effect, we developed a complete model for the flow-channel under the external applied pressure. Initial results from this model indicate that the fluid pressure induced change in the oil index accounted for the shift. More detailed modeling of this effect is under further investigation.

Results and Conclusions

Early channels demonstrated the detection of a linear relationship between refractive index changes and resonance wavelengths over a given wavelength interval regardless of their type. Experimentation with ring resonators was pursued because their display of large shifts would provide for small index change identification. The second generation of channels allowed the development of a method of obtaining real time data. Given the high quality factors (10^6) observed from the resonators and that subsequent readings varied by less than 1 pm, index sensitivity was 2.85×10^{-5} for this device. With optimized device, wavelength shift of nanometers and detection on a picometer scale will be achievable for true lab-on-chip applications.

Future Work

At the time of this paper, microring resonators attached to micospectrometers are being fabricated for real-time lab-on-chip analysis function. Surface functionalization with biotin for testing with the highly specific protein Streptavidin in real-time is also being pursued for a biological approach. Future plans include multiple protein detection on the same chip as well as chemical sensing.

Acknowledgements

I would like to express my appreciation to the NSF, National Nanotechnology Infrastructure Network Research Experience for Undergraduates Program, and the Georgia Institute of Technology for their funding and facilities. A special thanks to site coordinator Jennifer Tatham Root for a productive research environment. I would also like to express my gratitude to Dr. Ali Adibi and Dr. Siva Yegnanarayanan for inclusion in their research and to the MSMA Group and Photonics Research Group for their guidance.

References

- [1] De Vos, Katrien et alia, "Silicon-on-Insulator microring resonator for sensitive and label-free biosensing," *Opt. Express* 15, 7610-7615 (2007).

Development of Optical Fiber Packaging for Planar Lightwave Circuits by Microfabrication

Kylan Szeto

Physics, Rensselaer Polytechnic Institute

NNIN REU Site: Cornell NanoScale Science & Technology Facility, Cornell University

NNIN REU Principal Investigator: Prof. Michal Lipson, Electrical and Computer Engineering, Cornell University

NNIN REU Mentor: Dr. Carl Poitras, Electrical and Computer Engineering, Cornell University

Contact: szetok@rpi.edu, ml292@cornell.edu, cbp8@cornell.edu

Abstract/Introduction

Testing integrated sub-micrometer light guiding structures typically involves precisely nanopositioning tapered lens fibers to couple light into nanotapered waveguides [1]. This is done through optimization using piezoelectric stages and optical microscopes. While this method works well in a research environment, this time consuming and expensive process remains slow and impractical for packaging and makes it difficult to test waveguiding chips with multiple devices. More importantly, it makes it impractical for industry. This project proposes a solution by defining and etching trenches into the substrate in front of waveguides, in which inexpensive cleaved optical fibers are easily aligned and fixed in place with UV curable index matching epoxy. Cleaved fibers have a mode field diameter of about $8\ \mu\text{m}$, greatly reducing misalignment errors with sub-micrometer waveguides. This method involves etching trenches into silicon dioxide (SiO_2) and Si so that cleaved fibers can be easily aligned with the waveguides. The final phase of testing will measure the optical efficiency of light coupling into the chip's devices. This process is easily reproducible and offers a solution for mass production of integrated optical circuits.

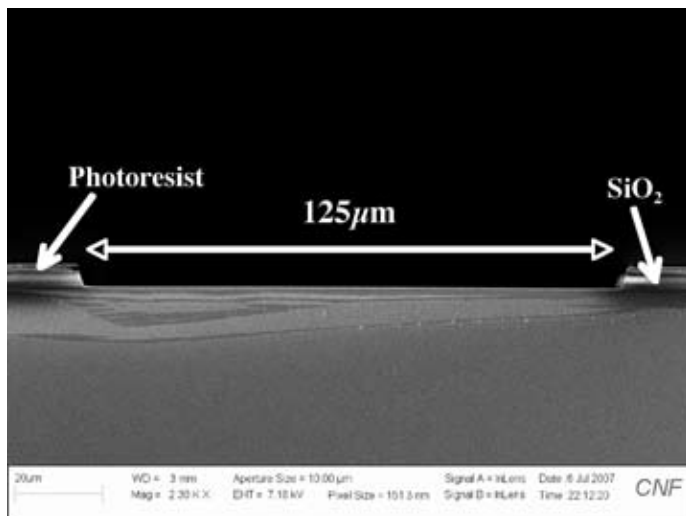


Figure 1: Oxide etch down to silicon substrate.

Experimental Procedure

The first phase of this project involved designing $125\ \mu\text{m}$ wide trench patterns to match the diameter of single mode SMF-28 optical fibers. A mask was created using the GCA/Mann 3600F optical pattern generator and used to characterize and define fabrication protocols on test Si wafers with a $3\ \mu\text{m}$ thick layer of thermally grown SiO_2 . By analyzing etch rates and selectivities of the Oxford 100 and Unaxis 770 etchers to SPR 220 photoresist, we decided to spin SPR 220-3.0 to a thickness of $3.3\ \mu\text{m}$. Characterization of the exposure dose for this thickness on the EV 620 contact aligner was best for 3 seconds using a 90 second MIF 300 development.

After photolithography, our wafer was subjected to a 20 second descum in the Glenn 1000 oxygen asher, and underwent $3\ \mu\text{m}$ of oxide etching in the Oxford 100 using the CHF_3/O_2 recipe for 35 minutes. This etch had to be characterized in order to determine how the trench profiles matched the desired dimension, as shown in Figure 1. Throughout fabrication, the depth of our trenches and etch rates were monitored using the F50 Filmetrics optical film measurement tool and the Tencor P10 profilometer.

Next we characterized the silicon etch with the Unaxis 770. This required 120 loops to remove the $59.5\ \mu\text{m}$ of Si, as shown in Figure 2.

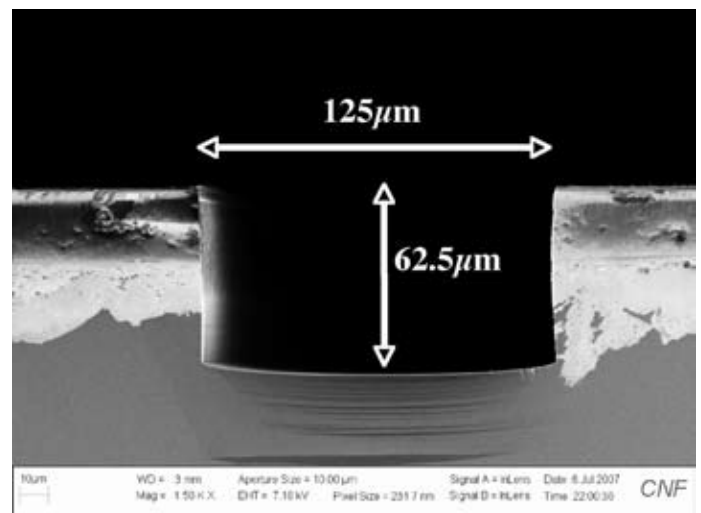


Figure 2: Deep etch into silicon substrate.

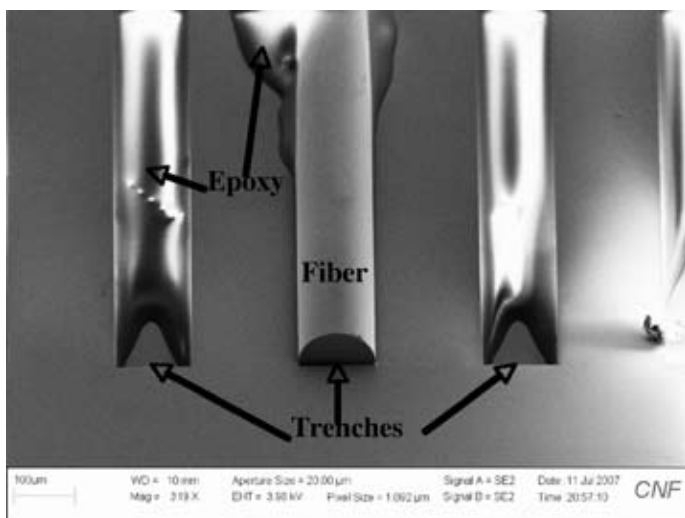


Figure 3: Dropped fiber held in place by epoxy.

The last steps were a hot resist strip and a 10 minute descum in the Glenn 1000. The wafer was then cleaved into individual chips, and a chip was mounted on a 3 axis rotation stage. Cleaved optical fibers were positioned using a 3 axis linear stage. Using this simple set up with an optical microscope we aligned and dropped fibers into the trenches. Finally, we glued them into place using UV curable index matching epoxy.

After mounting several fibers, we took scanning electron microscopy (SEM) images to characterize the position of the fibers (see Figure 3), and corrected our computer-aided design (CAD) to account for improper trench dimensions. We determined that $127 \mu\text{m}$ wide trenches with sacrificial trenches (epoxy drains) in between active sites were appropriate.

Our final step was to test these protocols on an SOI chip with waveguides, ring and disk resonators. After patterning the waveguides by e-beam lithography on an SOI sample, the devices were etched using the PT 770 and cladded with $2.8 \mu\text{m}$ of SiO_2 (GSI PECVD tool). We then spun $3.8 \mu\text{m}$ of resist onto our chip to account for the removal of the additional SiO_2 cladding, exposed our trench pattern using the ABM mask aligner for 9 seconds (used to expose small samples), and carried out the rest of the etch protocols as described above. We determined that the etch rates on both the Oxford 100 and the Unaxis 770 were much slower for small samples, but that the selectivities remained unchanged.

Results and Conclusions

The positioning of fibers into our functionalized chip was good, and the epoxy drains worked well; but this step was still sensitive to the epoxy drop size and placement. Also, trench and waveguide alignment was not accurate due to deterioration of alignment marks during e-beam lithography, forcing us to align the mask by eye (this problem can be easily resolved by adjusting the exposure doses of the alignment marks). After fixing fibers onto

both ends of the chip, we used a broadband amplified spontaneous emission light source and an Optical Spectrum Analyzer to test the devices. The best output graph is shown in Figure 4. This plot illustrates the resonant frequencies from the associated $8 \mu\text{m}$ ring resonator. This plot is also evidence that dropping optical fibers into pre-aligned trenches can be used to achieve good transmission, showing that this method is applicable for testing devices.

Future Work

Continued work should be put into perfecting the epoxy step to prevent defunctionalizing adjacent waveguides, or the need to space them far apart. Alternatively, further research into the use of multi-fiber systems such as ribbon fiber could prove beneficial. The ability to pre-space waveguides, drop, and epoxy many fibers simultaneously would greatly add to the efficiency of the drop-fiber method.

Acknowledgments

I would like to thank Professor Michal Lipson for the research opportunity in her lab, and Dr. Carl Poitras for providing me with the knowledge, and encouragement to complete my project. I'd also like to thank the Cornell Nanophotonics Research Group for all of their help. Special thanks to Ms. Melanie-Claire Mallison and Dr. Lynn Rathbun for making my experience the best it could be. Finally I'd like to thank the National Nanotechnology Infrastructure Network Research Experience for Undergraduates Program and the National Science Foundation for their funding.

References

- [1] Almeida, V; Panepucci, R; Lipson, M; "Nanotaper for Compact Mode Conversion"; Optics Letters, Vol. 28 No. 15, pages 1301-1304, August 1, 2003.

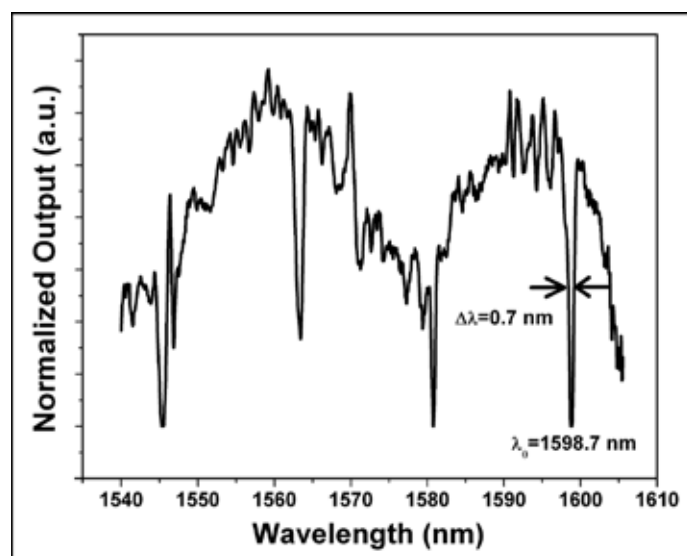


Figure 4: Power output graph from coupling tests.